Isotope Substitution Extends the Lifetime of Organic Molecules in Transmission Electron Microscopy

Thomas W. Chamberlain, Johannes Biskupek, Stephen T. Skowron, Peter A. Bayliss, Elena Bichoutskaia,* Ute Kaiser,* and Andrei N. Khlobystov*

Structural characterisation of individual molecules by high-resolution transmission electron microscopy (HRTEM) is fundamentally limited by the element and electron energy-specific interactions of the material with the high energy electron beam. Here, the key mechanisms controlling the interactions between the e-beam and C–H bonds, present in all organic molecules, are examined, and the low atomic weight of hydrogen—resulting in its facile atomic displacement by the e-beam—is identified as the principal cause of the instability of individual organic molecules. It is demonstrated theoretically and proven experimentally that exchanging all hydrogen atoms within molecules with the deuterium isotope, and therefore doubling the atomic weight of the lightest atoms in the structure, leads to a more than two-fold increase in the stability of organic molecules in the e-beam. Substitution of H for D significantly reduces the amount of kinetic energy transferred from the e-beam to the atom (main factor contributing to stability) and also increases the barrier for bond dissociation, primarily due to the changes in the zero-point energy of the C–D vibration (minor factor). The extended lifetime of coronene-d_{12}, used as a model molecule, enables more precise analysis of the inter-molecular spacing and more accurate measurement of the molecular orientations.

T. W. Chamberlain, S. T. Skowron, P. A. Bayliss,
E. Bichoutskaia, A. N. Khlobystov
School of Chemistry
The University of Nottingham, University Park
Nottingham NG7 2RD, UK
E-mail: elena.bichoutskaia@nottingham.ac.uk;
andrei.khlobystov@nottingham.ac.uk

J. Biskupek, U. Kaiser
Electron Microscopy of Materials Science
Central Facility for Electron Microscopy
Ulm University
Albert Einstein Allee 11
Ulm 89081, Germany
E-mail: ute.kaiser@uni-ulm.de

A. N. Khlobystov
Nottingham Nanotechnology & Nanoscience Centre
University of Nottingham
University Park
Nottingham NG7 2RD, UK

1. Introduction

Aberration-corrected high-resolution transmission electron microscopy (AC-HRTEM) has the potential to become a powerful method for imaging individual molecules with atomic resolution. AC-HRTEM provides complete structural information about the whole molecule, not just its surface, with the spatial resolution reaching the sub-Ångstrøm scale. Atomically thin carbon structures such as graphene,[1–4] graphene oxide[5–7] or single-walled carbon nanotubes (SWNT)[8–14] have been demonstrated as excellent substrates for molecules, providing mechanical support, efficient reduction of ionisation and suppression of molecular motion, thus enabling atomically resolved AC-HRTEM analysis at the single-molecule level.

These latest achievements illustrate the potential of AC-HRTEM to rival traditional spectroscopic methods of structural characterisation of molecular materials, provided that a crucial obstacle related to the invasive and destructive nature
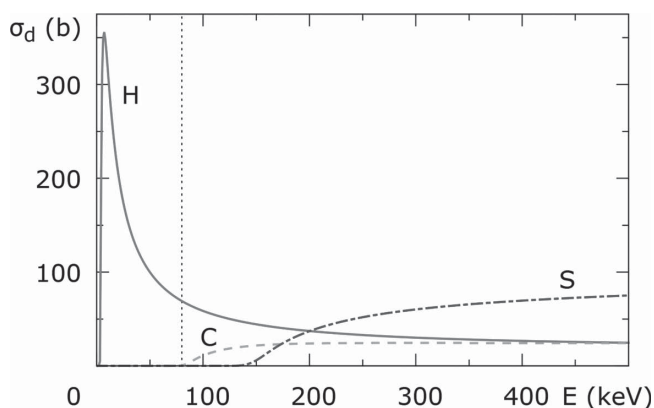
Figure 1. Ejection cross sections, σ_d (in barn), as a function of kinetic energy of the electron beam, E (in keV), for protium isotope of hydrogen (solid line), carbon (dashed line) and sulphur (dashed-dotted line), calculated for sulphur and hydrogen terminated graphene nanoribbons as example structures.[25] Notice that upon reduction of the e-beam energy the stability of carbon and other elements within a molecule increases while the stability of hydrogen atoms decreases sharply.

of the electron beam (e-beam) is overcome. The elastic forward scattering of the accelerated electrons of the e-beam by atoms of the sample molecules provides the main contribution to the imaging signal in HRTEM, however it can also cause so-called knock-on damage manifested in the ejection of atoms from the molecules, which typically leads to decomposition of the intrinsic structure faster than AC-HRTEM images can be captured.[15,16] To interpret experimental knock-on damage, the important quantity to consider is the ejection cross-section of an atom in the molecule, σ_d, which depends strongly on the kinetic energy of incident electrons (**Figure 1**), a fraction of which will be transferred to the atom in an elastic scattering event.[17–19] At an e-beam energy of 200 or 300 keV, commonly utilised in TEM, light and medium atomic weight elements that constitute the vast majority of molecular compounds are highly susceptible to ejection. However, a sharp decrease of σ_d for most elements when the energy of the e-beam is lowered[20] has the consequence that most of the studies on carbon-based materials in an aberration-corrected TEM are nowadays performed at voltages of 80 kV or 60 kV[21,22] and even below.[23,24]

For example σ_d for sp^2-carbon within graphitic structures approaches zero at the e-beam energy of about 80 keV (Figure 1) making it in principle possible to image carbon-based molecules using an e-beam set at or below this energy without perturbing their structures.[25] All other elements behave in a similar way to carbon under the e-beam, with the exception of hydrogen, which exhibits a dramatic increase in the ejection cross section at lower energies (Figure 1). While carbon and other elements within the molecule become more stable with reduction of the energy of the incident electrons, the probability of ejection of hydrogen atoms increases sharply. At and below 80 keV (optimum for carbon) H-atoms are removed instantaneously, thus making imaging of undamaged hydrogen-containing molecules by AC-HRTEM very challenging. The extreme discord of the σ_d for hydrogen with most other elements creates a fundamental barrier to atomic-resolution imaging of individual small organic molecules,

which represent building blocks for biomacromolecules[26–28] and molecular materials, such as polymers. In this study we provide a simple and elegant solution to this seemingly insurmountable challenge by substituting the most common protium isotope of hydrogen in organic molecules for the deuterium isotope. Isotopic substitution has no effect on the molecular structure but increases the atomic weight of the hydrogen atoms by 100% which drastically increases the stability of the molecules in the e-beam, allowing imaging of individual molecules.

2. Results and Discussion

It is important to explore the physical origin of the unusually large susceptibility of hydrogen atoms to knock-on damage by the e-beam. The classical Rutherford electron scattering cross-section describes the probability of an incident electron being elastically scattered by an atom:[29]

$$\sigma_R = \left(\frac{z \cdot e^2}{4\pi\varepsilon_0 \cdot 2 \cdot m_e \cdot c^2} \right)^2 \frac{1 - \beta^2}{\beta^4} \cdot CSC^4 \left(\frac{\theta}{2} \right) \tag{1}$$

where z is the nuclear charge, $\beta = v_e/c$ is the ratio of electron velocity v_e to the speed of light, c, θ is the electron scattering angle and m_e is the mass of an electron. The expression (1) was expanded[30] to improve the accuracy:

$$\sigma(\theta) = \sigma_R \left(1 - \beta^2 \sin^2 \left(\frac{\theta}{2} \right) + \pi \frac{ze^2}{\hbar c} \beta \sin \left(\frac{\theta}{2} \right) \left(1 - \sin \left(\frac{\theta}{2} \right) \right) \right) \tag{2}$$

The amount of kinetic energy T transferred from the incident electron to an atom in a collision leading to elastic scattering is expressed by the formula:

$$T = \frac{2 \cdot M \cdot E \left(E + 2m_e \cdot c^2 \right)}{\left(M + m_e \right)^2 \cdot c^2 + 2M \cdot E} \cdot \sin^2 \left(\theta / 2 \right), \tag{3}$$

where M is the mass of the atom, and E is the electron kinetic energy.

Generally, the atom is only ejected from the molecule by the e-beam, leading to irreversible knock-on damage, if the transferred energy T is greater than an ejection energy threshold, E_d, related to the strength of interatomic bonding within the molecule. The atom ejection cross-section can then be obtained by integrating σ expressed through T using Equations (2) and (3) in the energy range $T > E_d$:

$$\sigma_d = \int_{T > E_d} \sigma(T) \cdot \frac{4\pi}{T_{max}} dT = 4\pi \left(\frac{z \cdot e^2}{4\pi\varepsilon_0 \cdot 2 \cdot m_e \cdot c^2} \right)^2$$

$$\cdot \frac{1 - \beta}{\beta^4} \left\{ \frac{T_{max}}{E_d} - 1 - \beta^2 \cdot \ln \left(\frac{T_{max}}{E_d} \right) \right. \tag{4}$$

$$\left. + \pi \frac{z \cdot e^2}{\hbar \cdot c} \beta \left[2 \left(\frac{T_{max}}{E_d} \right)^{1/2} - \ln \left(\frac{T_{max}}{E_d} \right) - 2 \right] \right\}$$

where T_{max} is the maximum transferrable energy from the e-beam to an atom, which corresponds to $\theta = 180°$, and $\forall$ is
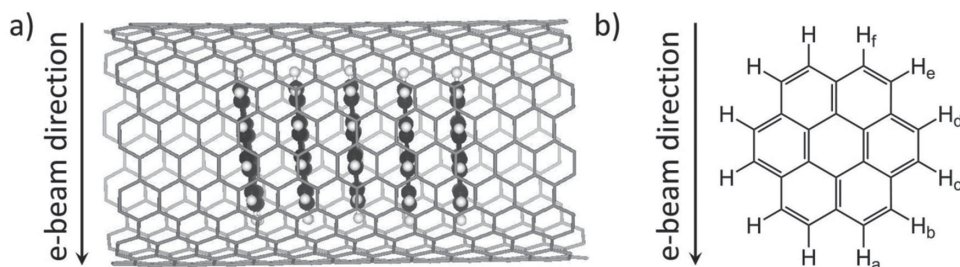
Figure 2. a) Coronene molecules stacked within a SWNT, b) which results in six non-equivalent C–H bonds (H_a- H_f) with respect to the electron beam.

the reduced Planck constant $h/2\pi$. This equation demonstrates that the stability of an atom to the e-beam has a complex dependence on both the nuclear charge and mass of the element (included in the T_{max} parameter) and the energy of the electron beam (included in β and T_{max}). The first term in Equation (4) resembles σ_R, which is proportional to z^2 of the atom: from this term alone lighter elements are expected to interact less with the e-beam, which may lead to the incorrect conclusion that lighter elements are less susceptible to knock-on damage. However, the effect of T_{max}, which is inversely proportional to atomic weight M, effectively counteracts the first term; significantly more kinetic energy is transferred from the e-beam to lighter atoms than heavier ones (Equation (3)). Ultimately, the balance between E_d and T_{max} is most important: if at a certain energy of the e-beam the maximum transferrable energy is below the ejection threshold, the chance of knock-on damage is zero ($\sigma_d = 0$) meaning that the molecule will be stable indefinitely during AC-HRTEM imaging. As hydrogen is the lightest element in the Periodic Table, the value of $T_{max}(H)$ is substantially higher than for other elements (compare $T_{max}(^1H) = 188$ eV and $T_{max}(C) = 16$ eV under an 80 keV e-beam). σ_d for hydrogen does not reach zero or any reasonably low value at any energy of the e-beam (Figure 1), which makes TEM imaging of structurally intact organic molecules practically impossible.

This analysis proves that the lack of stability of hydrogen atoms in molecules under the e-beam is related primarily to the low atomic weight of the H-atoms. One way to address this problem and therefore increase the stability of organic molecules in the e-beam is to replace the protium isotope of hydrogen in the molecule with heavier isotopes. Substitution of naturally abundant hydrogen (>99.9% ^1H protium isotope) for deuterium D (^2H isotope) which contains an additional neutron, doubles the atomic weight of a D-atom with respect to ^1H. The structure and chemical properties of deuterated organic molecules are thus identical to their ^1H analogues, but their stability in the e-beam should be significantly enhanced due to a lowering of the T_{max} parameter and thus an overall decrease of σ_d. In many cases isotope exchange readily takes place when organic molecules are treated with heavy water D_2O, offering a universal methodology for stabilising organic molecules for AC-HRTEM imaging.

To illustrate this principle, coronene was chosen as a model molecule as it has been studied by TEM previously[31–35] and is observed to decompose very fast upon e-beam irradiation at energies of 80–120 keV.[32] The

disk-like shape of coronene is easily recognisable in AC-HRTEM images and spontaneously forms stacks within the nanotube cavity, orienting molecular planes parallel to the direction of the e-beam (**Figure 2**a, and further on below). Although all 12 C–H bonds in coronene are chemically equivalent, the e-beam affects H-atoms in different ways depending on the angle between the individual C–H bond and the e-beam, leading to different values of E_d (Figure 2b).

Ab initio molecular dynamics (AIMD) has been used to calculate the values of E_d for ejections of hydrogen and deuterium atoms from coronene. These simulations demonstrate that the bonds parallel to the e-beam, such as C–H_a and C–H_f (see Figure 2b), are more susceptible to e-beam damage than other bonds. For protium isotope these bonds have the lowest ejection threshold of $E_d(H) = 6.1$ eV as the momentum of the e-beam is transferred directly along the bonds. This makes them the weakest points in the molecule and the subsequent H loss is the trigger for decomposition of coronene. It is interesting that regardless of whether the momentum is transferred in the direction of bond contraction (as in the case of C–H_f) or bond stretching (as in the case of C–H_a), the value of E_d remains the same (**Figure 3**).

The isotopic substitution of hydrogen for deuterium leads to a nearly 30% increase in E_d, from $E_d(H) = 6.1$ eV in C–H_a bond to $E_d(D) = 7.8$ eV for the C–D_a bond, which is related to the decreased zero-point vibrational energy E_0 for C–D bonds, making them more difficult to break (this forms the basis for differences in reactivity between isotopes in chemistry):

$$E_0 = \frac{h}{4\pi}\sqrt{\frac{k}{\frac{M(C)\cdot M(H \, or \, D)}{(M(C)+M(H \, or \, D))}}} \tag{5}$$

where k is the force constant, and M is the atomic weight of carbon, protium or deuterium respectively.

Under the e-beam a marked difference between the C–D_a and C–D_f bonds is observed: while the e-beam can still break the C–D_a bond (albeit with lower probability than C–H_a), the energy transferred to the deuterium atom in the C–D_f bond does not ricochet to bond dissociation as in the case of C–H_f but effectively dissipates through the molecule, leading to temporary structural deformations with no irreversible damage (Figure 3). In addition, the bond dissociation mechanism of the C–D_a bond is different to that of the C–H_a bond. While in the case of the C–H_a bond the transferred energy leads to multiple bond stretches eventually
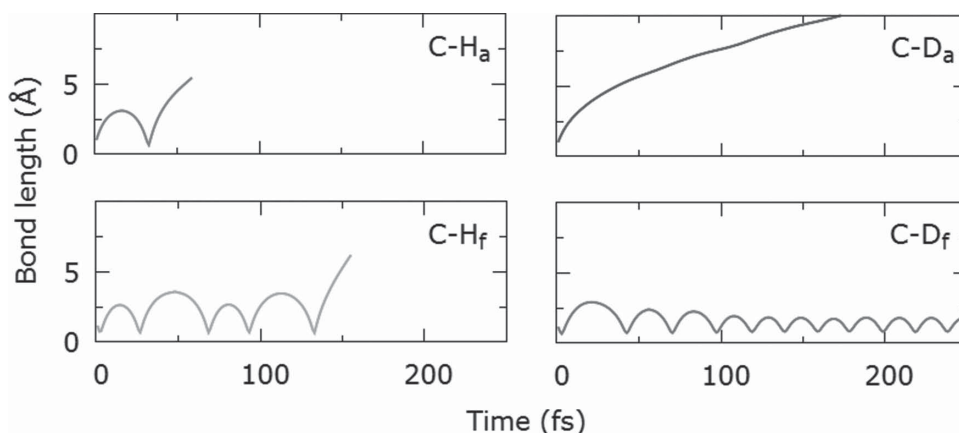
© 2014 Wiley-VCH Verlag GmbH & Co. KGaA, Weinheim

Figure 3. Variation of the C−H and C−D bond lengths with time calculated by AIMD after momentum corresponding to the E_d of C−H$_a$ ($E_d = 6.1$ eV) and C−D$_a$ ($E_d = 7.8$ eV) was transferred to the different protium atoms of coronene and the deuterium atoms of coronene-d$_{12}$ respectively. Bonds are broken in the cases of C−H$_a$, C−H$_f$ and C−D$_a$, but not C−D$_f$.

leading to dissociation, in the case of the C−D$_a$ bond the deuterium atom is removed directly with no contraction of the bond. Hence, both C−H$_a$ and C−H$_f$ bonds for coronene, and only C−D$_a$ bonds for coronene-d$_{12}$ are considered to be the most susceptible to knock-on damage, and as a result the cross sections associated with removal of these atoms were used to quantify the molecules stability in the e-beam.

A combination of the increase in the ejection threshold energy E_d and a significant decrease in the value of T_{max} has a profound impact on the ejection cross section σ_d for deuterium (**Figure 4**, dashed-dotted trace). For example, comparing the C−H$_a$ and C−D$_a$ bonds, the likelihood of ejection of deuterium is five times lower when compared to protium at the maximum of the cross section function (Figure 4).

It is instructive to compare the ejection cross sections of H and D in the range of e-beam energies between 80 and 100 keV because as the energy of e-beam decreases, the carbon framework of the molecules becomes infinitely stable in this range

(σ_d(C) → 0 just below 100 keV, Figure 3, inset). The cross-section of deuterium versus protium ejection from the most vulnerable bond in coronene is approximately 2.77 times higher at 80 keV and 2.74 times at 100 keV, indicating that deuterium can potentially withstand a nearly three times higher dose of electrons in the range of e-beam energies typically used for AC-HRTEM imaging compared to hydrogen.

In practical terms, the value of σ_d for the most easily broken chemical bond within a molecule and typical values of the e-beam dose rate j required for AC-HRTEM imaging can be used to estimate the time required for ejection of the first atom from the molecule (e.g. in the chemical kinetics terms, the ejection of first atom from coronene is likely to be a rate-controlling step for the decomposition of molecules within the stacks), t_{ev}, under the e-beam:[36]
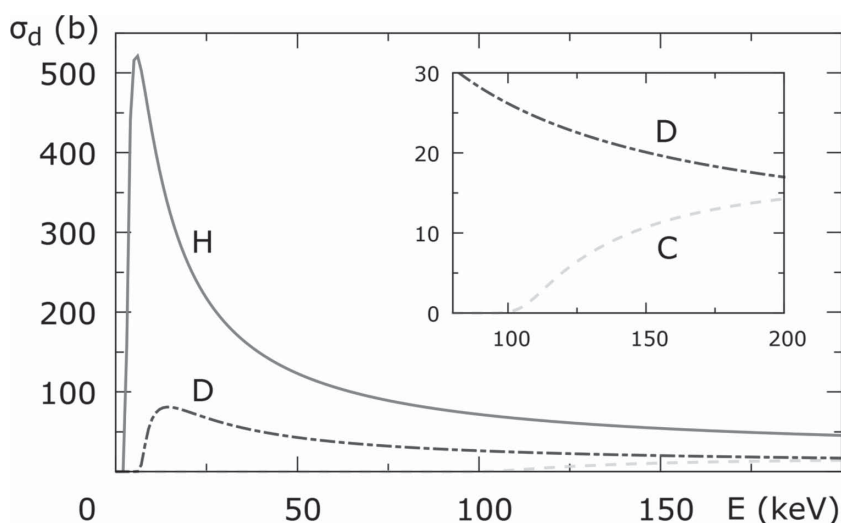
$$t_{ev} = \frac{1}{jn\sigma_d} \tag{6}$$

where n is the number of bonds of such type in the molecule. Considering that ejection of an atom from the organic molecule leads to highly reactive radical species causing rapid decomposition, t_{ev} gives a good estimate for the observed life-time of the molecule under the e-beam. Our calculations predict that under the same external conditions (same energy and dose rate of the e-beam) deuterated molecules should be 2–3 times more stable than the protium analogues, which should manifest in a 2–3-fold increase in the total e-beam dose they can tolerate and subsequently lead to a substantial increase in their lifetime under the e-beam (**Table 1**).

Figure 4. Ejection cross-sections, σ_d, as a function of electron beam kinetic energy E for protium (solid line), deuterium (dashed-dotted line) and carbon (dashed line) calculated for the C−H$_a$ and C−D$_a$ bonds in coronene and deuterated coronene. Inset shows σ_d of C and D at commonly used TEM e-beam energies of 80-200 keV.

Recent AC-HRTEM measurements on ^{13}C enriched graphene have recently enabled more accurate evaluation of cross section for the carbon lattice, but had only a marginal effect on the stability of graphene

Table 1. Ejection cross section (σ_d), time required for ejection of the first atom (t_{ev}), and total electron dose required for ejection of H, D and C atoms via knock-on damage in coronene and deuterated coronene calculated for different dose rates (j) of 80 or 100 keV e-beam.

Atom	Energy of e-beam [keV]	σ_d per atom [barn]	j [e-/barn/s]	t_{ev} [s]	Total e- dose [e/nm^2]
H	80	84.87	0.0001	59	$5.89 \cdot 10^7$
			0.0005	12	
	100	71.80	0.0001	70	$6.96 \cdot 10^7$
			0.0005	14	
D	80	30.59	0.0001	163	$1.63 \cdot 10^8$
			0.0005	33	
	100	26.18	0.0001	191	$1.91 \cdot 10^8$
			0.0005	38	
C	80	0.00	0.0001	∞	∞
			0.0005	∞	
	100	5.83×10^{-3}	0.0001	37015	$3.70 \cdot 10^{10}$

in the e-beam due to a relatively small difference in the atomic weights of ^{12}C and ^{13}C.[37] However, an alternative model describing the ejection of carbon atoms from graphene by a kinetic isotope effect (KIE) has recently been proposed which led to an unexpected conclusion that the graphene atomic lattice is extremely cold (~25 K) in the ambient temperature AC-HRTEM measurements.[38] Since KIE emanates primarily from the difference in the zero-point energies E_0 (Equation (5)) as illustrated by our calculations for C–H and C–D (Figure 3), it is therefore accounted for by the total cross sections function σ_d (Equation (4)) as a part of the E_d parameter. The description of molecular transformations under the e-beam by σ_d is all-inclusive (e.g. σ_d incorporates information about the zero-point energy for chemical bonds which determines KIE and other kinetic effects, as well as the amount of transferred energy from the e-beam to a particular atom and the likelihood of this transfer) and being mathematically rigorous it enables the accurate analysis and prediction of rates and pathways of transformations of molecules under the e-beam.

To verify this hypothesis and demonstrate its practical applicability, we prepared carbon nanotubes filled with stacks of coronene (coronene@SWNT) or deuterated coronene (coronene-d$_{12}$@SWNT) and compared their stability in the 80 keV e-beam. The protium atoms of coronene were exchanged for deuterium atoms in near-critical D$_2$O[40] and the degree of isotope exchange was confirmed by gas chromatography mass spectrometry to be >99%. Coronene and coronene-d$_{12}$ were encapsulated in carbon nanotubes from the gas phase using identical conditions, by heating the molecules and freshly opened SWNT at 400 °C in vacuum. Prior to AC-HRTEM analysis coronene@SWNT and coronene-d$_{12}$@SWNT samples were washed with toluene to remove any molecules from the surface of the nanotubes. The majority of nanotubes were densely filled with molecules in both cases (>95%), and the structures observed were essentially identical with the coronene and coronene-d$_{12}$ molecules both orientated at an angle of ~80° with respect to the nanotube sidewall (**Figure 5**).
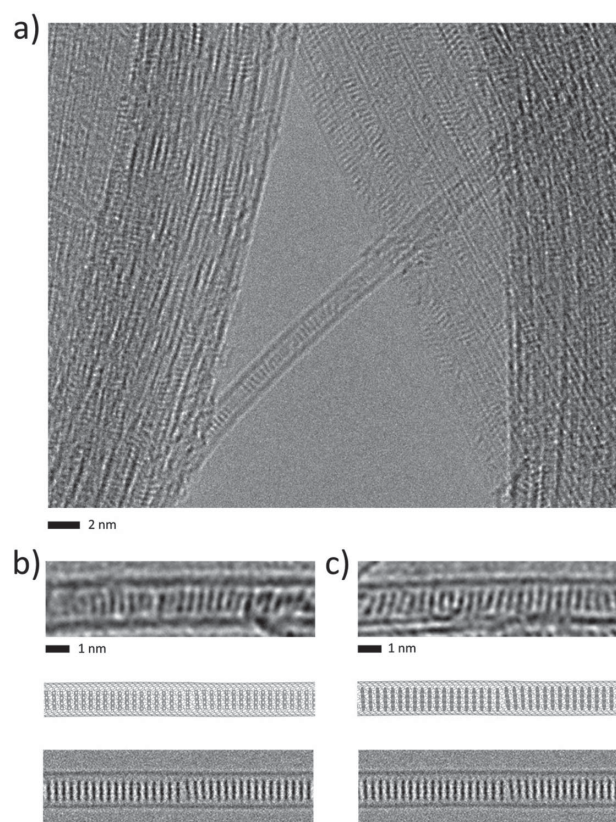

Figure 5. a) AC-HRTEM image of coronene-d$_{12}$@SWNT demonstrating excellent filling rates. b,c) Comparison of AC-HRTEM images, corresponding structural models and image simulations for coronene@SWNT (b) and coronene-d$_{12}$@SWNT (c) showing that the structures are essentially identical.

Qualitative AC-HRTEM observations indicate that coronene is significantly less stable in the e-beam, decomposing into amorphous featureless structures extremely quickly, so that extra care is needed (low e-beam dose rate and short exposure time) to obtain its images (Figure 5b), whereas coronene-d$_{12}$ (Figure 5c) appears to be significantly more stable. To quantify the enhancement in stability of C–D bonds with respect to C–H bonds, the dose rate of the 80 keV electron beam was set at $2 \cdot 10^5$ e$^-$/nm^2/s and time series images were recorded for both samples (**Figure 6**). Molecules of coronene and coronene-d$_{12}$ within the stacks were observed to decompose under the e-beam at different rates. The evolution of molecules in stacks was carefully monitored, and the cumulative dose of the e-beam required to destroy all molecules within the stack was recorded in each experiment, as described in the Experimental Section. A number of different areas were analysed for each sample and showed at least a two-fold increase in the stability of the deuterated molecules (**Table 2**). At a higher energy of 100 keV the difference in stability of coronene and coronene-d$_{12}$ is even more pronounced, with coronene decomposing almost instantaneously (ESI file).

The effects of isotope substitution were studied for crystals of coronene and coronene-d$_{12}$. About 20 crystals of each species were irradiated under identical imaging conditions and the loss of crystallinity was tracked as a function of dose rate by acquiring series of diffraction patterns (**Figure 7**). The
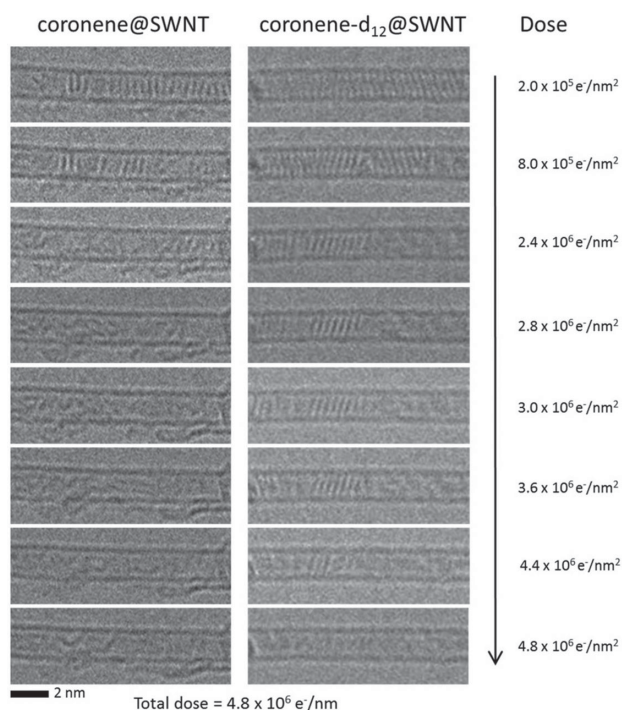
coronene@SWNT	coronene-d$_{12}$@SWNT	Dose

2.0 x 10^5 e$^-$/nm^2

8.0 x 10^5 e$^-$/nm^2

2.4 x 10^6 e$^-$/nm^2

2.8 x 10^6 e$^-$/nm^2

3.0 x 10^6 e$^-$/nm^2

3.6 x 10^6 e$^-$/nm^2

4.4 x 10^6 e$^-$/nm^2

4.8 x 10^6 e$^-$/nm^2

— 2 nm

Total dose = 4.8 x 10^6 e$^-$/nm

Figure 6. AC-HRTEM time series showing decomposition of coronene@SWNT (left) and coronene-d$_{12}$@SWNT (right) at 80 keV. All coronene molecules are decomposed due to knock-on damage by an e-beam dose of 2.8·10^6 e$^-$/nm^2 whilst coronene-d$_{12}$ molecules persist until a total dose of 4.8·10^6 e$^-$/nm^2.

experiments were always stopped at the point where no crystalline lattice reflections were visible and the irradiated areas were completely amorphous. In all measurements coronene-d$_{12}$ crystals appear to be a factor of >2.0 more stable than coronene to the 80 keV e-beam (Table 2). Considering that both types of crystals have virtually identical physicochemical properties (e.g. ionisation potential, thermal and electrical conductivity) this series of measurements demonstrates that the knock-on mechanism is likely to be the main source of damage of molecules in extended 3D crystal structures. This can be effectively controlled by isotopic substitution, extending lifetimes of molecules in crystals in similar fashion to that of chains of molecules confined in nanotubes.

The observed enhanced stability of deuterated molecules versus hydrogenated analogues, both inside of nanotubes and in the solid state as crystals, matches well our theoretical predictions (Table 1) and confirms the general principle that isotopic substitution of H for D can significantly extend the

Table 2. Observed total dose of the 80 keV e-beam required for the irreversible knock-on damage of coronene and coronene-d$_{12}$ molecules located within SWNT (averaged over 15 different areas for each sample) and in crystal state (averaged over 20 samples).

Structure	Average e-beam dose required for decomposition of molecules [e$^-$/nm^2]
coronene@SWNT	(4.1 ± 2.1) 10^6
coronene-d$_{12}$@SWNT	(7.4 ± 3.8) 10^6
coronene crystal	(1.2 ± 0.4) 10^4
coronene-d$_{12}$ crystal	(2.9 ± 1.0) 10^4

lifetime of organic molecules during imaging in a transmission electron microscope. Extended lifetime coronene-d$_{12}$ used as a model molecule in our studies enabled a more precise analysis of the inter-molecular spacing within the stack (0.39 ± 0.03 nm) and molecular orientations inside nanotubes (79.8 ± 4.6°), as compared to the shorter-lived coronene (0.4 ± 0.1 nm and 83 ± 4° respectively), and is consistent with previous studies.[31] In future the isotope substitution stabilisation can be applied to organic and bio-organic molecules with unknown complex structures which can be determined by AC-HRTEM imaging.

3. Conclusions

In this study we demonstrate that the amount of kinetic energy transferred from the electron beam to hydrogen atoms (the lightest chemical element), ubiquitously present in all organic molecules, is the major obstacle to single-molecule structural characterisation by transmission electron microscopy. We have identified the extremely low atomic weight of hydrogen as the principal cause of its instability in TEM, and demonstrated theoretically and proved experimentally that exchange of protium isotope for the heavier deuterium (doubling the atomic weight) can lead to a more than two-fold increase in stability of organic molecules under HRTEM imaging conditions. Our isotope substitution methodology coupled with improvements to e-beam sources, electromagnetic lenses and electron detectors, is a large step towards non-invasive structural analysis of individual molecules in a transmission electron microscope, which can now be applied to more complex organic and biological structures.

4. Experimental Section

Computational Methods: All AIMD simulations were performed as described in a previous study,[25] using B3LYP/6-31G level of theory. The initial atomic velocities in the AIMD simulations were randomly sampled from a Maxwell-Boltzmann distribution at 298 K, which was also used to calculate the thermal lattice contributions to the cross-sections.

Materials Preparation: Coronene-d$_{12}$ was prepared by treating coronene using conditions reported previously.[39] IR spectroscopy and mass spectrometry confirmed product formation and the degree of deuteration was determined via GC-MS to be >99%.

SWNT (arc-discharge, P2-SWNT, Carbon Solutions Ltd) were heated at 500 °C for 20 minutes in air. Coronene or coronene-d$_{12}$ (15 mg) was mixed with the SWNT (5 mg), sealed under vacuum (10^{-6} mbar) in a Pyrex glass ampoule and heated at 400 °C for 3 days. The sample was allowed to cool and was then washed to remove excess molecules from the exterior of the SWNT by suspending in toluene (20 mL) with ultrasonication followed by filtration through a PTFE membrane (0.2 µm pore size) to give coronene@SWNT and coronene-d$_{12}$@SWNT samples as a black powder.

Transmission Electron Microscopy: TEM specimens were heated in air at 150 °C for 7 min shortly before insertion into the
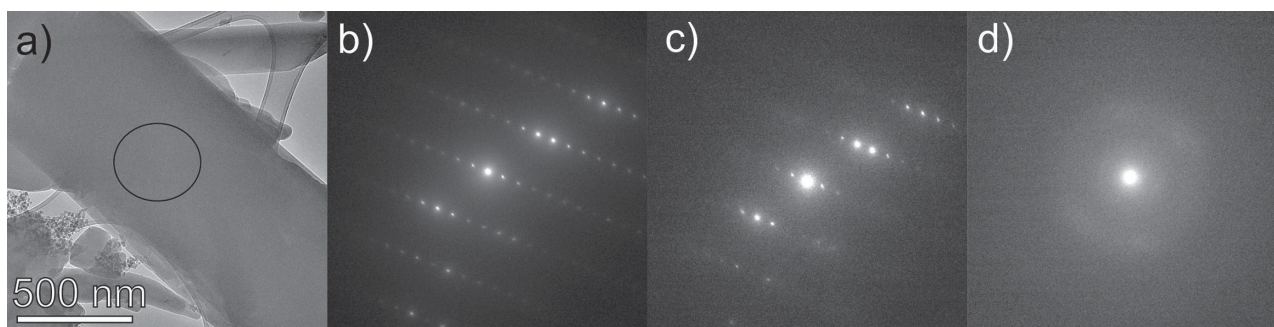
Figure 7. Diffraction patterns of a selected area of coronene-d_{12} crystal (a, indicated by the circle) at the start of the irradiation with the 80 keV e-beam (b), after an accumulated dose of $2.0 \cdot 10^4$ e$^-$/nm^2 (c, most of the reflections disappeared due decay and disorder of molecules in the crystal) followed complete amorphisation after $3.8 \cdot 10^4$ e$^-$/nm^2 (d).

TEM column. The aberration-corrected HRTEM imaging was carried out using an image side C_s-corrected FEI Titan 80–300 transmission electron microscope operated at 80 kV acceleration voltage with modified filament extraction voltage for enhancements of contrast and information limit.[40] Images were recorded on a slow-scan CCD-camera type Gatan Ultrascsan XP1000 (FEI Titan) using the pre-specimen beam-blanker to avoid electron irradiation during the camera read-out time. 100 kV imaging was performed on a JEOL2100 FEG TEM. For all in-situ irradiation experiments the microscope provided a highly controlled source of local and directed electron radiation on a selected area of the sample. The electron flux was kept to a minimum whilst searching for a suitable area, focussing and stigmating the lens, with the total search dose was between 2–$6 \cdot 10^5$ e$-$/nm^2, this corresponds to an accumulated dose typically used for 1 to 3 normal image acquisitions and does not contribute significantly (less than 5–10%) to the total dose used for the comparison of stabilities of coronene and coronene-d_{12} (Figure 6). For irradiation experiments the applied electron-flux was kept constant at $2 \cdot 10^5$ e$^-$/nm^2/s, and the total applied dose was approximately in the order of up to $1 \cdot 10^7$ e$^-$/nm^2 at the end of each HRTEM experiment. Electron diffraction patterns of coronene and coronene-d_{12} crystals were acquired using 80 keV electrons and a low dose rate of 190 e$^-$/nm^2/s. A selected area aperture (50 µm) was applied to record a diffraction pattern from specified sample areas that covered an irradiated area of about 300 nm in diameter. All experiments were carried out at room temperature.

TEM image simulations were carried out using the multi-slice program QSTEM.[41] The structure models were based on a (10,10) SWNT filled with either coronene or coronene-d_{12}. The electrostatic scattering potential is identical for H and D atoms, however, the mass of the atoms varies and therefore the phonon configuration. The different phonon configurations were considered by using different Debye-Waller factors (14.2 Å^{-2} for H, resp. 7.1 Å^{-2} for D) and averaging each time 30 TDS (thermal diffuse scattering) frozen phonon configurations. The general calculation parameters of the image simulation have been chosen according to the experimental settings: voltage 80 kV, spherical aberration 10 µm, focus -7.4 nm (corresponds to Scherzer-focus with black atom contrast), focus spread 4 nm. A limited electron dose of $2 \cdot 10^5$ e$^-$/nm^2 was considered by applying Poisson-distributed noise derived from a subsequent Monte-Carlo simulation. The dampening of the CCD camera was included by applying the modulation transfer function (MTF) to the intensity distribution of the exit wave.

[1] R. S. Pantelic, J. C. Meyer, U. Kaiser, H. Stahlberg, *Solid State Commun.* **2012**, *152*, 1375.
[2] A. Chuvilin, U. Kaiser, E. Bichoutskaia, N. A. Besley, A. N. Khlobystov, *Nature Chem.* **2010**, *2*, 450.
[3] F. Schaffel, M. Wilson, J. H. Warner, *ACS Nano* **2011**, *5*, 9428.
[4] N. P. E. Barry, A. Pitto-Barry, A. M. Sanchez, A. P. Dove, R. J. Procter, J. J. Soldevila-Barreda, N. Kirby, I. Hands-Portman, C. J. Smith, R. K. O'Reilly, R. Beanland, P. J. Sadler, *Nature Commun.* **2014**, DOI:10.1038/ncomms4851.
[5] R. S. Pantelic, J. C. Meyer, U. Kaiser, W. Baumeister, J. M. Plitzko, *J. Structural Biology* **2010**, *170*, 152.
[6] R. S. Pantelic, J. W. Suk, C. W. Magnuson, J. C. Meyer, P. Wachsmuth, U. Kaiser, R. S. Ruoff, H. Stahlberg, *J. Structural Biology* **2011**, *174*, 234.
[7] J. Sloan, Z. Liu, K. Suenaga, N. R. Wilson, P. A. Pandey, L. M. Perkins, J. P. Rourke, I. J. Shannon, *Nano Lett.* **2010**, *10*, 4600.
[8] T. W. Chamberlain, J. C. Meyer, J. Biskupek, J. Leschner, A. Santana, N. A. Besley, E. Bichoutskaia, U. Kaiser, A. N. Khlobystov, *Nature Chem.* **2011**, *3*, 732.
[9] M. D. Gimenez-Lopez, A. Chuvilin, U. Kaiser, A. N. Khlobystov, *Chem. Commun.* **2011**, *47*, 2116.
[10] A. Chuvilin, A. N. Khlobystov, D. Obergfell, M. Haluska, S. H. Yang, S. Roth, U. Kaiser, *Angew. Chem. Int. Ed.* **2011**, *49*, 193.

[11] C. S. Allen, Y. Ito, A. W. Robertson, H. Shinohara, J. H. Warner, *ACS Nano* **2011**, *5*, 10084.

[12] Z. Liu, K. Yanagi, K. Suenaga, H. Kataura, S. Iijima, *Nature Nanotechnol.* **2007**, *2*, 422.

[13] M. Koshino, Y. Niimi, E. Nakamura, H. Kataura, T. Okazaki, K. Suenaga, S. Iijima, *Nat. Chem.* **2010**, *2*, 117.

[14] E. Bichoutskaia, Z. Liu, N. Kuganathan, E. Faulques, K. Suenagal. J. Shannon, J. Sloan, *Nanoscale* **2012**, *4*, 1190.

[15] R. F. Egerton, *Ultramicroscopy* **2013**, *127*, 100.

[16] R. F. Egerton, *Microscopy Res. Technique* **2012**, *75*, 1550.

[17] D. Cherns, F. J. Minter, R. S. Nelson, *Nucl. Instrum. Methods* **1976**, *132*, 369.

[18] R. F. Egerton, R. McLeod, F. Wang, M. Malac, *Ultramicroscopy* **2010**, *110*, 991.

[19] L. W. Hobbs, in Introduction to Analytical Electron Microscopy (Eds: J. J. Hren, J. I. Goldstein, D. C. Joy), Plenum Press, New York **1987**, pp.399–445.

[20] T. Susi, J. Kotakoski, R. Arenal, S. Kurasch, H. Jiang, V. Skalakova, O. Stephan, A. V. Krasheninnikov, E. I. Kauppinen, U. Kaiser, J. C. Meyer, *ACS Nano* **2012**, *6*, 8837.

[21] R. Zan, U. Bangert, Q. M. Ramasse, K. S. Novoselov, *J. Phys. Chem. Lett.* **2012**, *3*, 953.

[22] T. Zoberbier, T. W. Chamberlain, J. Biskupek, N. Kuganathan, S. Eyhusen, E. Bichoutskaia, U. Kaiser, A. N. Khlobystov, *J. Am. Chem. Soc.* **2012**, *134*, 3073.

[23] K. Suenaga, Y. Iizumi, T. Okazaki, *Eur. Phys. J. Appl. Phys.* **2011**, *54*, 3350.

[24] U. Kaiser, J. Biskupek, J. C. Meyer, J. Leschner, L. Lechner, H. Rose, M. Stöger-Pollach, A. N. Khlobystov, P. Hartel, H. Müller, M. Haider, S. Eyhusen, G. Benner, *Ultramicroscopy* **2011**, *111*, 1239.

[25] S. T. Skowron, I. V. Lebedeva, A. M. Popov, E. Bichoutskaia, *Nanoscale* **2013**, *5*, 6677.

[26] X.-C. Bai, I. S. Fernandez, G. McMullan, S. H. Schere, *eLife* **2013**, *2*, e00461.

[27] X. Li, P. Mooney, S. Zheng, C. R. Booth, M. B. Braunfeld, S. Gubbens, D. A. Agard, Y. Cheng, *Nature Methods* **2013**, *10*, 584.

[28] M. Liao, E. Cao, D. Julius, Y. Cheng, *Nature* **2013**, *504*, 107.

[29] A. Zobelli, A. Gloter, C. P. Ewels, G. Seifert, C. Coliex, *Phys. Rev. B* **2007**, *75*, 245402.

[30] W. McKinley, H. Feshbach, *Phys. Rev.* **1948**, *74*, 1759.

[31] T. Okazaki, Y. Iizumi, S. Okubo, H. Kataura, Z. Liu, K. Suenaga, Y. Tahara, M. Yudasaka, S. Okada, S. Iijima, *Angew. Chem. Int. Ed.* **2011**, *50*, 4853.

[32] B. Botka, M. E. Füstös, H. M. Tóháti, K. F. Németh, G. Klupp, Z. Szekrényes, D. Kocsis, M. Utczás, E. Székely, T. Váczi, G. Tarczay, R. Hackl, T. W. Chamberlain, A. N. Khlobystov, K. Kamaras, *Small* **2014**, *10*, 1369.

[33] A. V. Talyzin, I. V. Anoshkin, A. V. Krasheninnikov, R. M. Nieminen, A. G. Nasibulin, H. Jiang, E. I. Kauppinen, *Nano Lett.* **2011**, *11*, 4352.

[34] A. I. Chernov, P. V. Fedotov, A. V. Talyzin, I. S. Lopez, I. V. Anoshkin, A. G. Nasibulin, E. I. Kauppinen, E. D. Obraztsova, *ACS Nano* **2013**, *7*, 6346.

[35] M. Fujihara, Y. Miyata, R. Kitaura, Y. Nishimura, C. Camacho, S. Irle, Y. Iizumi, T. Okazaki, H. Shinohara, *J. Phys. Chem. C* **2012**, *116*, 15141.

[36] A. Santana, A. Zobelli, J. Kotaksoki, A. Chuvilin, E. Bichoutskaia, *Phys. Rev. B* **2013**, *87*, 094110.

[37] J. C. Meyer, F. Eder, S. Kurasch, V. Skalakova, J. Kotakoski, H.-J. Park, S. Roth, A. Chuvilin, S. Eyhusen, G. Benner, A. Krasheninnikov, U. Kaiser, *Phys. Rev. Lett.* **2012**, *108*, 196102.

[38] K. Harano, S. Takenada, S. Okada, Y. Niimi, N. Yoshikai, H. Isobe, K. Suenaga, H. Kataura, M. Koshino,E. Nakamura, *J. Am. Chem. Soc.* **2014**, *136*, 466P.

[39] C. Boix, M. Poliakoff, *Tetrahedron Lett.* **1999**, *40*, 4433.

[40] J. Biskupek, P. Hartel, M. Haider, U. Kaiser, *Ultramicroscopy* **2012**, *116*, 1.

[41] C. T. Koch, PhD thesis, Arizona State University (2002). (The program is available at http://elim.physik.uni-ulm.de).